Crystal Structure of Human D-Dopachrome Tautomerase, a Homologue of Macrophage Migration Inhibitory Factor, at 1.54 Å Resolution[†,‡]

Hiroshi Sugimoto,[§,||] Masae Taniguchi,[§] Atsushi Nakagawa,[§,⊥] Isao Tanaka,[*,§,⊥] Masaki Suzuki,[#] and Jun Nishihira[#]

Division of Biological Sciences, Graduate School of Science, Hokkaido University, Sapporo 060-0810, Japan, and Central Research Institute, School of Medicine, Hokkaido University, Sapporo 060-0815, Japan

Received September 10, 1998; Revised Manuscript Received December 15, 1998

ABSTRACT: D-Dopachrome tautomerase shares a low homologous amino acid sequence (33% homology) with the macrophage migration inhibitory factor (MIF) and possesses similar tautomerase activity as well. MIF is a cytokine involved in inflammatory reactions and immune responses. Whereas recent studies have identified MIF as a pituitary hormone and immunoregulator, much less is known about the structural basis of these physiological functions and the real significance of tautomerase activity. Therefore, interest in the structure−function relationship between D-dopachrome tautomerase and MIF has increased, especially with regard to inflammation and immune responses. We have determined the X-ray crystal structure of human D-dopachrome tautomerase at 1.54 Å resolution. D-Dopachrome tautomerase folds to form a homotrimer that has extensive contact between subunits by intersubunit β-sheets. Its overall topology and trimeric formations are similar to those of human MIF. The N-terminal proline is located at the bottom of a positively charged pocket in which the conformations of Lys32 and Ser63 are highly conserved. These positively charged properties are also seen in the active site pocket of human MIF, bacterial 5-(carboxymethyl)-2-hydroxymuconate isomerase (CHMI), and 4-oxalocrotonate tautomerase (4-OT). A detailed comparison of these structures revealed significant differences in the environment around the potential active site, the intersubunit contacts, and charge distribution on the molecular surface. It can be concluded that these features are related to the physiological role and tautomerase activity of MIF and D-dopachrome tautomerase. The present structural study could be helpful for designing effective inhibitors that modulate immunoregulatory and hormone-like effects.

An enzyme that converts 2-carboxy-2,3-dihydroindole-5,6-quinone (D-dopachrome) into 5,6-dihydroxyindole (Scheme 1) was unexpectedly found during an investigation of L-dopachrome tautomerization activity in melanogenesis of cultured melanoma cells (*1*). This 13 kDa enzyme was isolated from rat livers and referred to as D-dopachrome tautomerase. The molecular cloning of D-dopachrome tautomerase cDNA has shown little amino acid sequence homology with L-dopachrome tautomerase (TRP-1 or TRP-2), which catalyzes isomerization of L-dopachrome to 5,6-dihydroxyindole-2-carboxylic acid (*2, 3*). Recently, there has been great interest in the physiological role of D-dopachrome tautomerase. This protein was found to share a homologous amino acid sequence with MIF[1] (Figure 1), which is known to be profoundly involved in a broad spectrum of inflammatory and immunological events (*4*).

Scheme 1

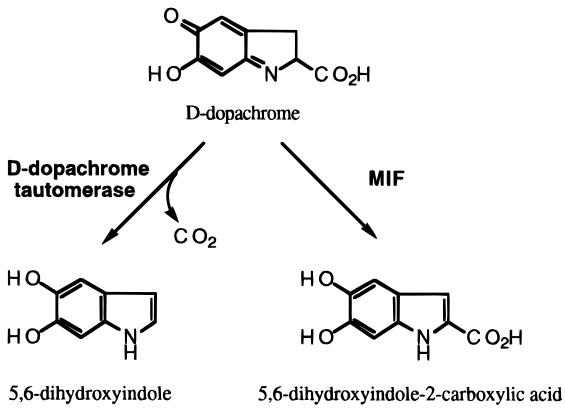

MIF was originally identified as a cytokine released from activated T-lymphocytes (*5, 6*); it plays a pivotal role in septic shock and delayed-type hypersensitivity (*7, 8*). Recently, this protein was rediscovered as a macrophage-derived cytokine and as a hormone released by the anterior pituitary gland in response to inflammatory stimuli (*7, 9, 10*). Calandra et al. have shown that a significant amount of MIF is secreted

[†]This work was supported by a Grant-in-Aid for the Ministry of Education, Science and Culture of Japan (No. 09670144) and by the Research for the Future Program (JSPS-RFTF 97L00501) from the Japan Society for the Promotion of Science.

[‡] The atomic coordinates and observed structure factors of D-dopachrome tautomerase have been deposited in the Brookhaven Protein Data Bank (ID codes 1dpt and r1dptsf).

* To whom correspondence should be addressed. Phone: +81-11-706-3221. Fax: +81-11-706-4905. E-mail: tanaka@polymer.sci.hokudai.ac.jp.

[§] Graduate School of Science, Hokkaido University.

[||] Research fellow of the Japan Society for the Promotion of Science.

[⊥] Members of the TARA project of Tsukuba University, Japan.

[#] School of Medicine, Hokkaido University.

[1] Abbreviations: MIF, macrophage migration inhibitory factor; CHMI, 5-(carboxymethyl)-2-hydroxymuconate isomerase; TRP, tyrosinase-related protein; PEG, poly(ethylene glycol); 4-OT, 4-oxalocrotonate tautomerase; LPS, lipopolysaccharide; GSH, glutathione; GST, glutathione *S*-transferase; 3-BP, 3-bromopyruvate.

10.1021/bi982184o CCC: $18.00
Published on Web 02/20/1999

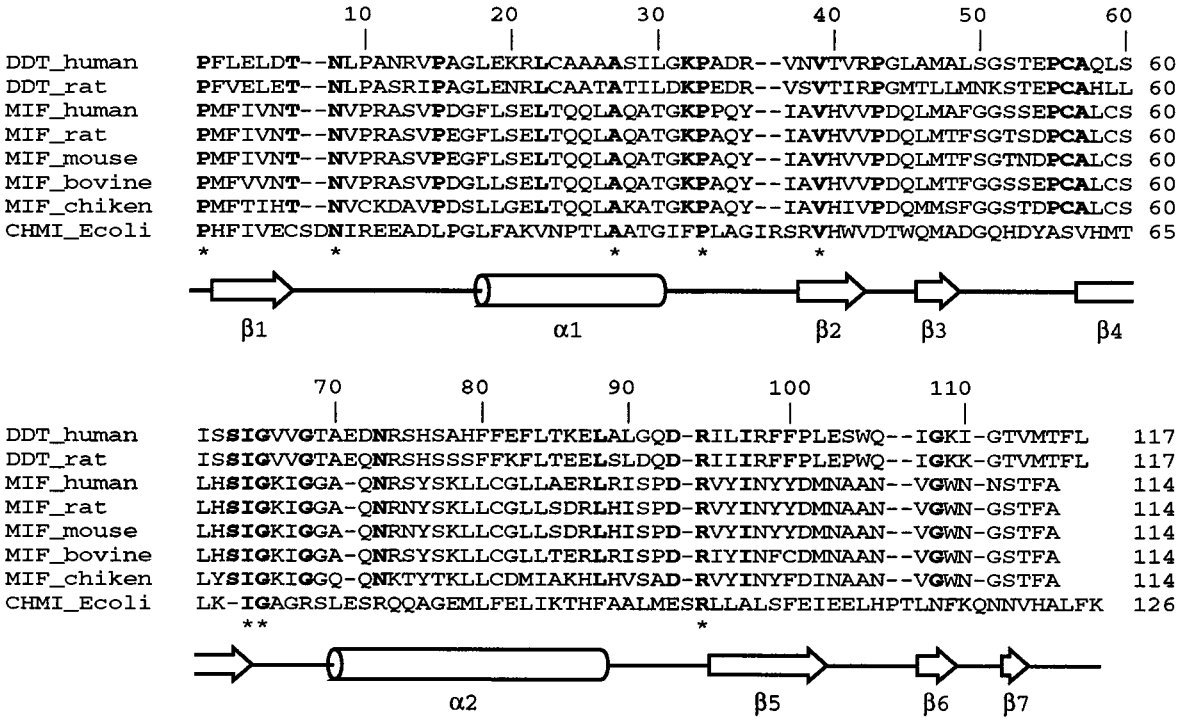

FIGURE 1: Sequence alignment of human D-dopachrome tautomerase with rat D-dopachrome tautomerase, five MIF, and *E. coli* CHMI. The secondary structure of human D-dopachrome tautomerase is shown. Elements of the secondary structures are indicated by α for α-helix and β for a strand of β-sheet. The sequence identity of human D-dopachrome tautomerase and human MIF and CHMI is 33% and 17%, respectively. Invariant residues among D-dopachrome tautomerase and MIF are shown in bold type. Invariant residues are marked by asterisks.

from the pituitary gland and that this protein has the potential to counterregulate the antiinflammatory action of glucocorticoid (*11*). Moreover, an array of immunohistochemical studies revealed the expression of MIF in various tissues, including the embryonic chicken lens, which suggests that MIF not only functions as an immunoregulatory protein but also acts as a cell differentiation factor as well as a hormone (*12*−*17*).

A few research groups, including ours, have presented reports on the tertiary structure of MIF (*18*−*21*) and demonstrated that it forms a homotrimer with three β-sheets surrounded by six α-helices. The structure shares a common architecture with the bacterial enzymes 5-(carboxymethyl)-2-hydroxymuconate isomerase (CHMI) and 4-oxalocrotonate tautomerase (4-OT) (*22*). Although the sequence alignment between MIF and CHMI shows relatively low homology (18%), these two proteins have almost identical subunit topology with two $\beta\alpha\beta$ motifs linked by pseudo-2-fold symmetry in the monomers and trimeric packing by intersubunit β-sheets.

It is of interest that the N-terminal proline residue is well conserved among MIF, CHMI, 4-OT (*18*), and D-dopachrome tautomerase. Recently, MIF and D-dopachrome tautomerase were identified as enzymes catalyzing the tautomerization of D-dopachrome (*23*) (Scheme 1) and phenyl pyruvate (*24*), which are unlikely to be the true substrates for MIF and D-dopachrome tautomerase because of their low affinities to these substrates. Although a recent report shows the relation between cytokine activity and enzymatic reaction (*25*), the physiological significance of tautomerase activity is still under debate. Nonetheless, previous findings suggest some functional and evolutionary relationship between D-dopachrome tautomerase and MIF. In this context, it appears that a comparative study of the protein structures of these substances would be helpful in order to further understand the biological functions of both D-dopachrome tautomerase and MIF.

METHODS

Crystallization and Data Collection. Human D-dopachrome tautomerase cDNA was cloned and overexpressed in *Escherichia coli* (*26*). Purification, crystallization, and preliminary crystallographic analysis of D-dopachrome tautomerase were performed as described previously (*27*). In brief, the crystals were grown in hanging drops by mixing 3 μL of reservoir solution [23% (w/v) PEG 4000, 0.1 M sodium citrate, pH 5.7, and 0.2 M ammonium acetate] with 3 μL of protein solution (10 mg/mL in 100 mM Tris-HCl, pH 7.8). The crystals grew to a size of approximately $0.3 \times 0.3 \times 0.2$ mm^3 in 1 week at 18 °C. They belonged to the tribunal space group $P3$ with cell constants of $a = b = 84.2$ Å and $c = 41.0$ Å. There are three monomeric molecules in an asymmetric unit. X-ray diffraction data of the native crystals were collected from a single crystal at room temperature using a Fuji imaging plate detector with a Rigaku IPR-4080 imaging scanner and a Weissenberg camera for macromolecular crystallography (*28*) on BL-6B at the Photon Factory, KEK, Japan. Integrated intensities were obtained with DENZO (*29*) and were reduced using the CCP4 package (*30*). The overall merging R-factor was 3.6% for 104 959 observations of 43 724 reflections between 20 and 1.54 Å resolution. The data are 90.9% complete with an $\langle I/\sigma(I)\rangle$ of 15.4. In the highest resolution shell (1.54−1.62 Å), the data set was 81.9% complete with a merging R-factor of 0.276. The Se-Met crystals were obtained by microseeding under similar conditions, in which small crystals of the native

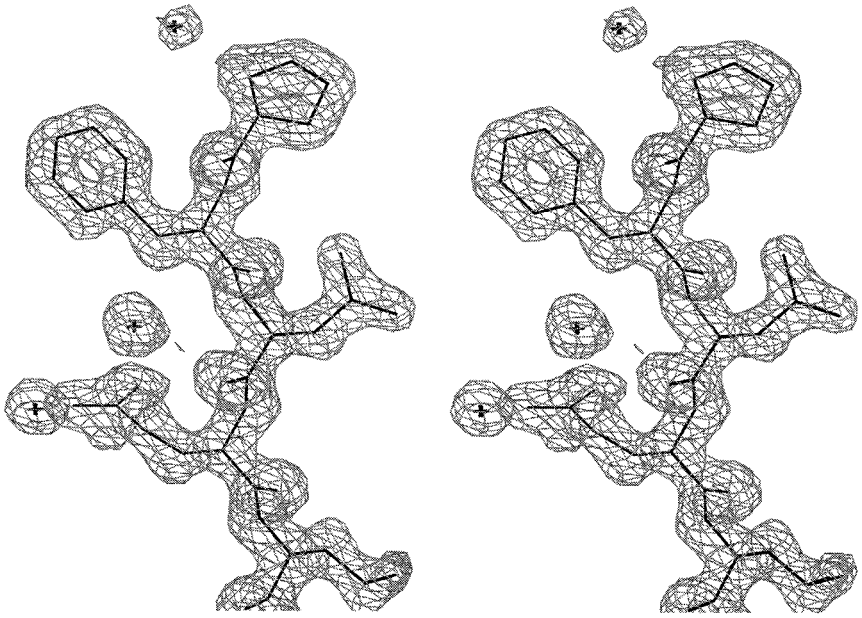

FIGURE 2: Final electron density [sigmaA (*61*) weighted $2F_o - F_c$ map] superimposed upon the model that had been refined to 1.54 Å. The region around Pro1 is shown contoured at 1.2σ using program O (*37*).

protein were used for seeding. Data of Se-Met crystals were collected at room temperature on BL-6A at the Photon Factory.

Molecular Replacement. The initial model of human D-dopachrome tautomerase was obtained by molecular replacement using the program AMoRe (*31*). A search model was constructed from the atomic coordinates of human MIF (*19*). The correct solution could not be obtained using either the monomer or trimer of MIF or their polyalanine model as the molecular probe. It was, however, possible to find a solution when the search model was constructed on the basis of sequence alignment. Thirty-three residues that were identical in both human D-dopachrome tautomerase and human MIF were retained, and the others were replaced with alanine. The rotation and translation functions were calculated using the native data (8−4 Å resolution), which yielded three molecules in an asymmetric unit with a correlation coefficient of 0.205 and an *R*-factor of 0.554. Each molecule generated an MIF-like trimer by crystallographic 3-fold symmetry. The refinement of the parameters on rotation and translation by AMoRe gave a correlation coefficient of 0.689 and an *R*-factor of 0.466. Then the side chains of the model were replaced to reflect those of D-dopachrome tautomerase. The temperature factors of atoms in MIF were kept in the molecular probe using the SEAMAN program (*32*). The solution by molecular replacement was refined as a rigid body by the program X-PLOR (*33*); this was done to further improve the orientation and positional parameters, which resulted in an *R*-factor of 0.485 for the data at 8−3 Å resolution.

Refinement. The model was submitted to simulated annealing refinement (*34*) using slow-cool protocols (*35*) from 3000 to 300 K with the data at 8−2 Å. Noncrystallographic symmetry (NCS) restraints were used for all atoms. At this stage, the crystallographic *R*-factor and a free *R*-factor (*36*) dropped to 0.333 and 0.352, respectively. Calculation of the $2F_o - F_c$ map was of good quality, and the main chain traces of residues Glu71, Phe116, and Leu117, which were not included in the molecular probe, could be easily recognized by inspecting $2F_o - F_c$ and $F_o - F_c$ maps. Selenium D Fourier synthesis with the phase of this model confirmed the solution, in which the six highest peaks were in good agreement with the expected sulfur atoms in methionine residues of the model. Subsequent cycles of rebuilding [manual model fitting using the program O (*37*)] followed by positional refinement and thermal parameter refinement with X-PLOR were used to improve the model, as judged by the free *R*-factor. Then the high-resolution limit of the diffraction data was increased from 2.0 to 1.54 Å by increments of 0.1 Å.

At the final stage of X-PLOR refinement, a slight NCS restraint was used, and the low-resolution limit of the diffraction data was increased from 8.0 to 20.0 Å by applying a bulk solvent correction (*38*). The positions of water molecules that were greater than 3.0σ in $F_o - F_c$ maps were identified automatically using PEAKMAX and WATPEAK. The peaks that formed reasonable hydrogen bonds to protein atoms or water molecules were included in the model by inspection of the electron density map. Analysis of the protein geometry was performed with the programs PROCHECK (*39*) and WHAT CHECK (*40*). All main chain dihedral angles were within the allowed (97.0%) or additional allowed (3.0%) regions of the Ramachandran plot. Figure 2 shows the final electron density map at 1.54 Å resolution superimposed upon the final model. The refined model included all residues (1−117) in each chain and 248 water molecules, yielding an *R*-factor of 0.164 and a free *R*-factor of 0.192. The rms deviations in bond lengths and angles were 0.008 Å and 1.4°, respectively. A summary of the refinement statistics is given in Table 1.

RESULTS AND DISCUSSION

Overall Structure. Figure 3 shows an α-carbon trace for the human D-dopachrome tautomerase monomer. Each of the three monomers contained in an asymmetric unit forms a functional trimer related by crystallographic 3-fold symmetry of the space group *P*3. Thus, it was calculated that three independent trimers of D-dopachrome tautomerase exist

Table 1: Final Refinement Statistics

parameter	
program	X-PLOR 3.851
resolution range (Å)	20.0−1.54
no. of reflections[a]	43,723
R-factor[b]	0.164
free *R*-factor	0.192
no. of non-hydrogen atoms	
protein	2655
water	248
average *B* values (Å^2)	
main chain	11.39
side chain	15.25
protein, all atoms	13.21
water molecules	31.51
all atoms	14.77
bulk solvent parameters	
k_{sol} (electron/Å)	0.3226
B_{sol} (Å)	72.69
estimated error on atomic position[c] (Å)	0.14
rms deviation from ideality	
bonds (Å)	0.008
angle (deg)	1.4
dihedral angle (deg)	27.3
improper angle (deg)	0.82

[a] The test set that was not used in the refinement of the model was randomly selected as 4% of data. [b] $R = \sum_h||F_o(h)| - |F_c(h)||/\sum_h F_o(h)$, where F_o and F_c are the observed and calculated structure factor amplitudes, respectively. [c] Estimated from the Luzzati plot (*41*).

per unit cell (Figure 4A). In the crystal, all of the trimers are stacked head to tail along the *c*-axis of the unit cell. The three chains are essentially identical to each other in tertiary structure. Only the surface region of the B chain is rather different from the others, especially in the helix α1. This deviation appeared to be due to the crystal packing. When the cell is projected along the *c*-axis, the orientations of three independent trimers are almost identical. However, the direction of one trimer which is comprised of the B chain opposes the other two (Figure 4A). The B chain exists in a different packing environment. A superposition for all 117 Cα atoms in the A, B, and C chains in the asymmetric unit gives rms deviations of 0.180, 0.096, and 0.138 Å for fitting B onto A, A onto C, and B onto C, respectively. These deviations are approximately equal to the coordinate error (0.14 Å), which was estimated from a Luzzati plot (*41*) for the refined structure.

Figure 5A shows that each monomer is composed of two α-helices (labeled α1 and α2) and seven β-strands (labeled β1−β7). These secondary structural elements can be grouped into three parts: (1) the central region which contains two βαβ motifs consisting of mixed four-stranded β-sheets with two antiparallel helices that run almost parallel with the 3-fold axis; (2) the β3 region (residues 46−49), flanked on one side of the central region, joining the intersubunit β-sheet; and (3) the C-terminal region (β6, residues 105−108, and β7, residues 111−113) on the opposite side of the β3 region, also joining to another intersubunit β-sheet. There is a pseudo-2-fold axis in the monomer running perpendicular to the β-sheet.

A large hydrophobic core exits in the central part of the monomer. A number of hydrophobic residues are located between the β-sheets and the two α-helices; most of the side chains (β1, Leu3 and Leu5; β2, Val37, Val39, and Val41; β4, Ile59 and Ile61; β5, Ile95, Ile97, and Phe99) toward the helices participate in hydrophobic interactions in this region. Helices α1 and α2 also interact tightly with the hydrophobic residues (α1, Leu18, Leu22, Ala25, Ala26, and Ile29; α2, Phe80, Phe81, Phe83, and Leu84). Thus, the β-sheets and two α-helices form the hydrophobic core, and no space has been observed to be accessed by solvent molecules in this region of the crystal structure.

β3, apart from the central region, is in contact via hydrogen bonds with the β2 of an adjacent monomer (Figure 5A). The water molecules also contribute to the main chain conformation of the β3 region. The water connects from N and O of Met47 (which are located in the middle of the β3 strand) to Nδ2 of Asn8 (which belongs to the central part). This water molecule has a good hydrogen-bonding geometry and possesses a low-temperature factor. The β3 protrudes from the central part of monomer and is located on the surface of trimer molecules. These water-mediated hydrogen bonds play a role in maintaining the β-strand and flexible loops to make contact with the adjacent monomer.

In addition to the intersubunit hydrogen bonds and water-mediated hydrogen bonds, proline residues in the connecting loops also have significance. There are seven proline residues per monomer of human D-dopachrome tautomerase. Generally, proline prevents the N atom from participating in hydrogen bonding and does not allow the typical main chain conformations in the protein; proline plays a structurally very important role. In the present case, all of the prolines except Pro1 are in the connecting loop and are highly conserved among all species of D-dopachrome tautomerase and MIF. For this novel trimeric structure, these highly conserved proline residues may play a key role in peptide folding with the formation of intersubunit β-sheets.

The C-terminal region is also separated from the central part of the human D-dopachrome tautomerase. The short two-stranded β-sheet consisting of β6 and β7 with a sharp β-turn (Lys109-Ile-Gly-Thr112) participates in the β-sheet of an adjacent monomer (Figure 5A). This region is located at the side of helix α2 of an adjacent monomer.

The crystal structure of D-dopachrome tautomerase shows trimer formation with exact 3-fold symmetry (Figure 5B). The β-sheet in the central region of one monomer is linked to the β3 strand of an adjacent monomer and to β6-β7 of another adjacent monomer. Thus, it forms seven-stranded β-sheets within a trimer. The formation of β-sheets by three monomers provides the principal contacts that stabilize the trimer structure. The relationship among complex secondary structure elements in the trimer is the same as that observed in human MIF (*19*) (see below).

The overall shape of the trimer structure is cylindrical along the 3-fold axis with approximate dimensions of 50 Å in diameter and 40 Å axial in length. There is a channel running up the 3-fold axis. The channel narrows in the middle and becomes wider near its edge. Both edges are surrounded by hydrophobic residues (Phe100, Pro101, and Leu102 at the bottom of the channel; Ala11, Val41, Pro43, and Leu45 are at the top). However, there are clusters of polar (Thr40, Ser62, and Gln58) and charged (Glu4, Asp6, Arg42, and Arg98) side chains in the middle of the channel. Most contacts across the trimer interfaces are lined by hydrogen bonds which afford the β-sheet structure. However, the side chains of Arg42, Leu100, and Phe101 are close to their symmetry-related atoms in the channel. The narrowest point is located at the side chain of Arg42, less than 2.5 Å from

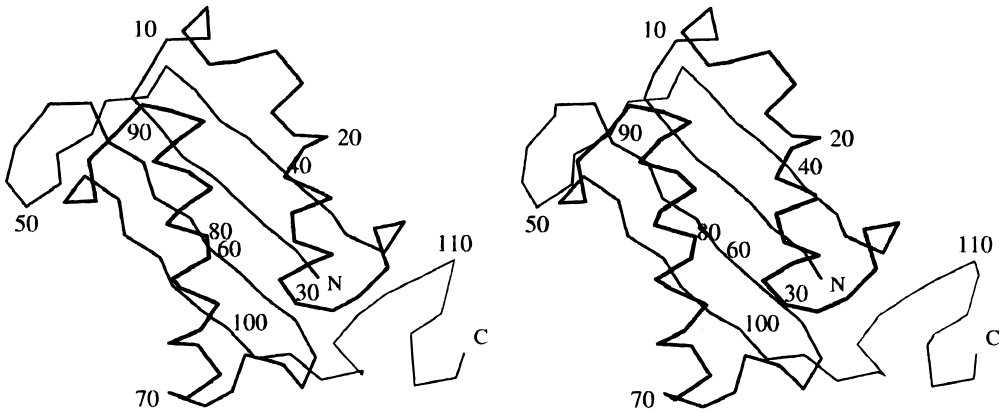

FIGURE 3: Stereopair of a Cα trace of the structure for the human D-dopachrome tautomerase monomer. Every tenth Cα atom is labeled. The figure was prepared with MOLSCRIPT (*62*).

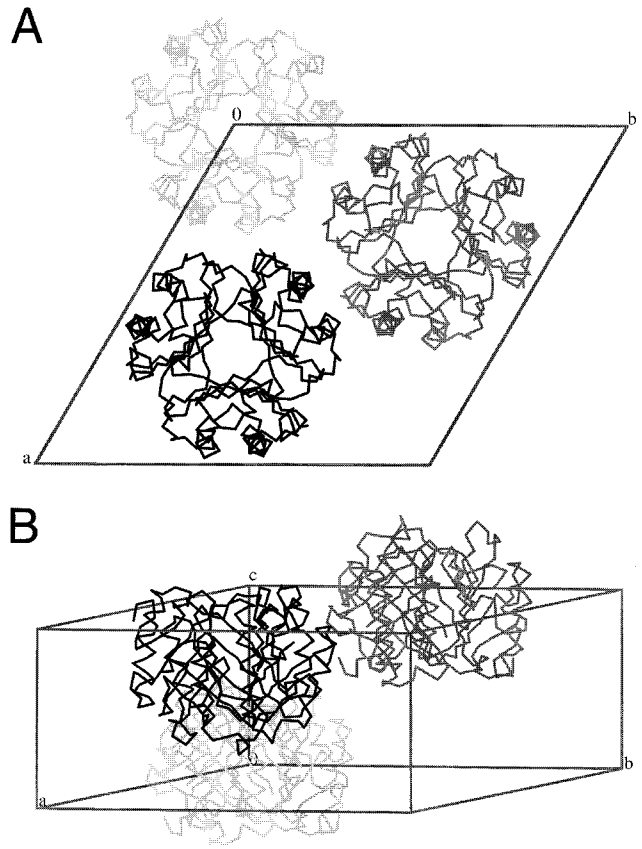

FIGURE 4: Crystal packing arrangement of human D-dopachrome tautomerase. (A) Three independent trimers of D-dopachrome tautomerase exist per unit cell. Each of the three monomers contained in an asymmetric unit forms a functional trimer related by crystallographic 3-fold symmetry. Each trimer molecule is colored in gray (A chain), black (B chain), or dark gray (C chain). When the cell is projected along the *c*-axis, the orientation of three independent trimers is almost identical. (B) The direction of the trimer of the B chain is opposite to the other two. In the crystal, all of the trimers are stacked head to tail along the *c*-axis of the unit cell.

the 3-fold axis. Therefore, the triplet Arg42 side chain is associated with van der Waals interactions, which would further contribute to the stability of the trimer formation. Although it is unlikely that any solvent molecule would be capable of passing through the channel, more than 10 water molecules per monomer are linked by hydrogen bonding to the side chain of the channel. The thermostability of this protein (*42*) may be due to these features, as well as to the tightly packed hydrophobic core, which is a result of the large number of hydrophobic residues between the β-sheet and helices.

Comparison with MIF. Recently, MIF was found to have enzymatic activity, converting D-dopachrome to 5,6-dihydroxyindole-2-carboxylic acid (*23*). This novel action gave rise to the challenging question of whether this particular enzyme activity is directly or indirectly involved in biological actions described in previous reports such as immunomodulation and proinflamatory effects. To investigate these possibilities, a comparative structural study between MIF and D-dopachrome tautomerase must have significant results. As demonstrated in the present study, overall folding and a subunit topology of human D-dopachrome tautomerase are almost identical to human MIF (*19*), with two βαβ motifs related by pseudo-2-fold symmetry and similar trimeric β-sheet packing (Figures 6 and 7). Briefly, when the α-carbons in strands β1, β2, β4, and β5 (residues 2−7, 38−42, 57−64, and 95−102) of the D-dopachrome tautomerase monomer are superimposed with the structurally corresponding atoms (residues 2−7, 38−42, 57−64, and 94−101) of human MIF, the rms difference is less than 0.57 Å at each chain (Figure 6A). A superposition for triad β-sheets in the trimer results in an rms difference of less than 0.95 Å. The backbone conformations of several connecting loops are also similar to those of MIF.

The hydrophobic cores between the β-sheets and helices in the monomer are highly conserved in both D-dopachrome tautomerase and MIF. Although the relative positions of helices are changed along the 3-fold axis and the angle between helix α1 and α2 is different (by 9°), many hydrophobic side chains comprise the core of this region. Among the 19 hydrophobic residues contributing to hydrophobic interactions between the β-sheets and two helices, five of them are completely conserved and the remainder are substituted by amino acid residues having similar physicochemical properties.

The largest structural differences in the main chain conformation between D-dopachrome tautomerase and MIF exist in two regions. The first region is at helix 2 (α2), which shifts toward the end of the helix along its axis. This may be due to the insertion of Glu71 in D-dopachrome tautomerase, which is located at the second residue of α2. However, α2 shifts only by about 1 Å, maintaining its almost parallel direction to the 3-fold axis in the trimer. These data

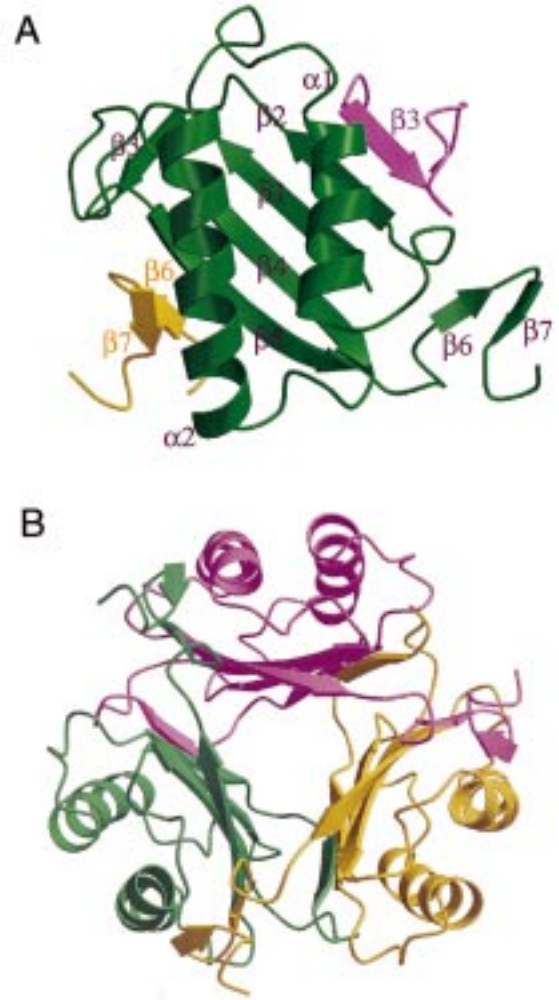

FIGURE 5: Crystal structure of human D-dopachrome tautomerase. (A) Schematic diagram of a human D-dopachrome tautomerase monomer and β-strands of an adjacent monomer. The monomer is colored green. The core of the monomer has a pseudo-2-fold axis running perpendicular to the plane of the β-sheet between β1 and β4. The β3 strand (residues 46−50) and the C-terminal β6 and β7 strands are almost perpendicular to strands β1, β2, β4, and β5. The four-stranded β-sheet in each monomer is hydrogen-bonded to an extra β-strand, β3, of the second monomer (purple) and to β6-β7 of the third monomer (yellow), forming an inter-monomer seven-stranded β-sheet. (B) Functional D-dopachrome tautomerase trimer viewed along the triad axis. This view is from the bottom side of (A). One monomer is colored green and two adjacent monomers related by crystallographic 3-fold symmetry are colored yellow and purple. The inside of the trimer is created by three β-sheets surrounded by six α-helices. These figures were prepared with MOLSCRIPT (*62*) and RASTER3D (*63*).

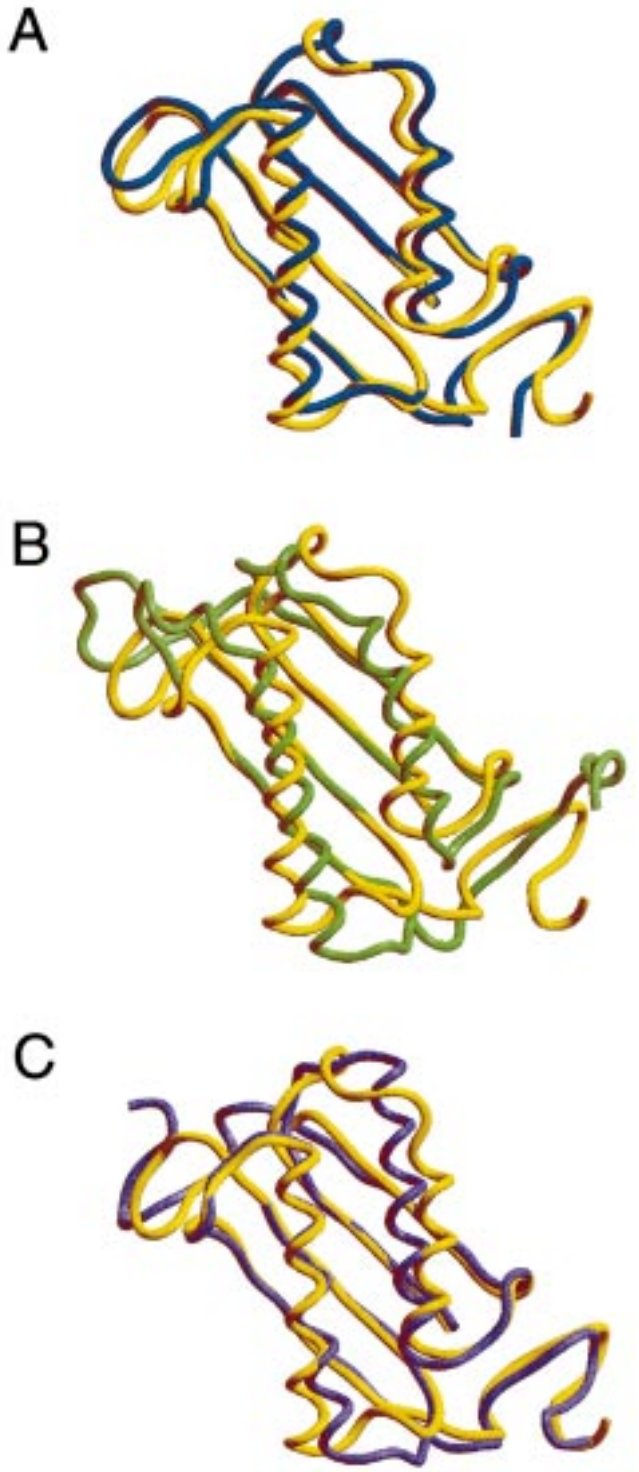

FIGURE 6: Structural comparison of human D-dopachrome tautomerase and several isomerases. Superposition of 27 α-carbon atoms at the four-stranded β-sheet of human D-dopachrome tautomerase monomer (yellow) on (A) human MIF (blue), (B) *E. coli* CHMI (green) (PDB code 1otg), and (C) *Pseudomonas* sp. CF600 4-OT (purple) (PDB code 1otf). The human D-dopachrome tautomerase monomer could be superimposed by least-squares fitting of 27 main-chain atoms of MIF, CHMI, and 4-OT monomers within an rms distance of 0.60, 0.88, and 0.72 Å, respectively. This figure was prepared with SETOR (*64*).

indicate that the very tight hydrophobic interaction between the β-sheet, α1, and α2 and the direction of α-helices are all important in this trimeric packing.

The second region is in the backbone conformation of the C-terminal tail. D-dopachrome tautomerase contains two extra residues in this region. The tail forms a small 3_{10}-helix by three residues (Met114−Phe116), which are exposed to the solvent although these residues have hydrophobic properties.

Furthermore, one of the greatest differences between the two proteins is observed in the surface residues. Representation of the molecular surface of both enzymes reveals that the overall shapes and electric properties are different, especially when viewed from the N-terminal side along the 3-fold axis. In the case of MIF, most of the surface of the bottom, shown in Figures 3 and 5A, including the potential active site pockets, is positively charged, and the region around the 3-fold axis is non- or negatively charged (Figure

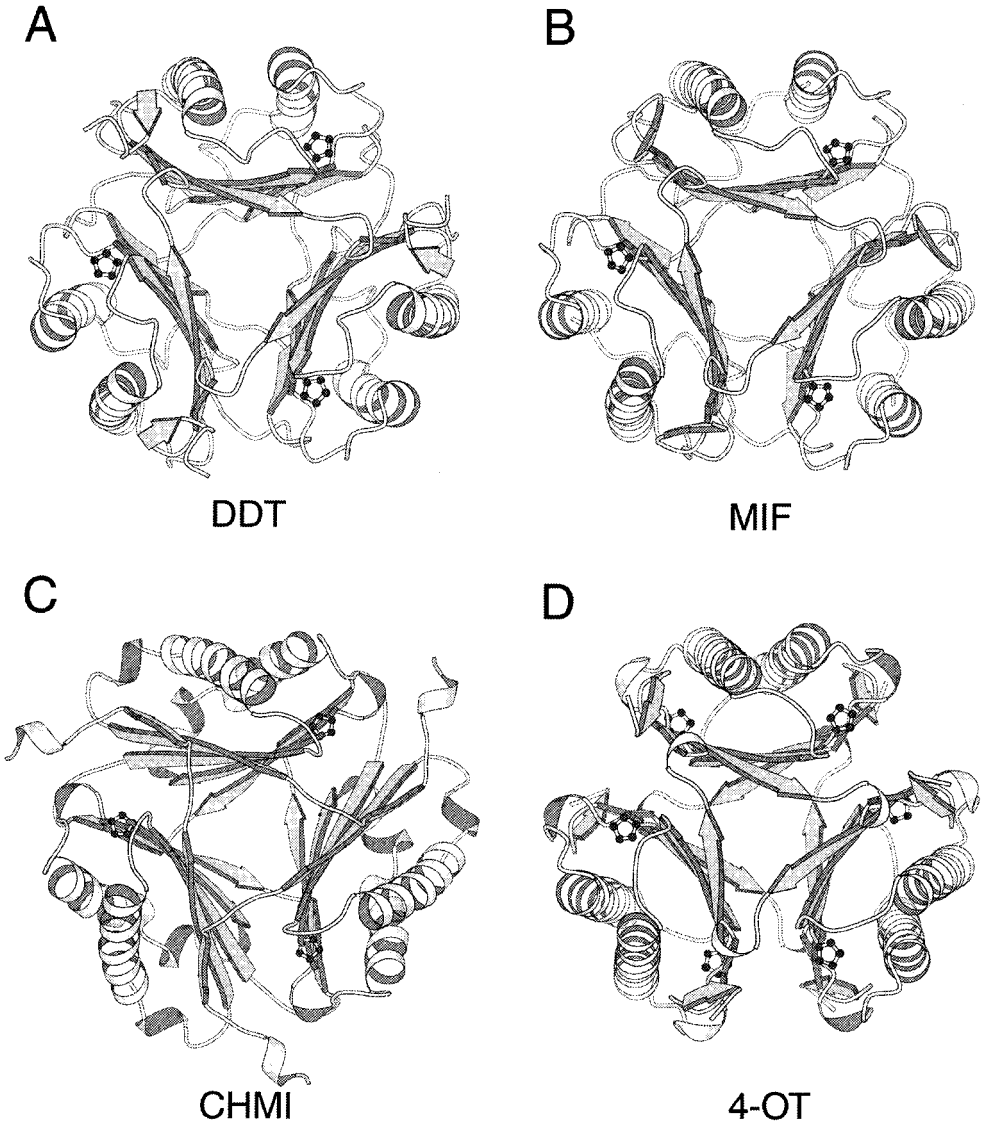

FIGURE 7: Ribbon representation of the (A) human D-dopachrome tautomerase trimer, (B) human MIF trimer, (C) CHMI trimer, and (D) 4-OT hexamer, viewed along the 3-fold axis. N-Terminal prolines are shown in a ball-and-stick representation. These figures were prepared with MOLSCRIPT (*62*).

8A). On the other hand, a negatively charged surface is widely distributed on the same side in the case of D-dopachrome tautomerase (Figure 8B). The relationship between this striking difference and biological activities is unclear at present. However, they share certain similarities in that there are small pockets at the potential active site and these regions are positively charged by the contribution of surface residues, including highly conserved Lys32 and the unconserved positively charged residue. These observations may reflect the fact that both proteins catalyze similar tautomerization reactions of substrate D-dopachrome. The invariant positively charged properties around the N-terminal pocket suggest that positively charged residues on the surface play an important role in the tautomerase reactions. The wide distribution of positive charges on the surface of MIF and the negative charges on that of D-dopachrome tautomerase must also be important for their biological actions.

The proposed active site of MIF for tautomerization is the hydrophobic pocket close to the N-terminal proline residue. Swope et al. reported that the P1G mutant of MIF reduces both the cytokine activity and enzymatic activity (*25*), suggesting that the N-terminal proline in the pocket must be a key to understanding the physiological role of these proteins. Pro1 of MIF, which may serve as a catalytic base, is surrounded by many aromatic residues (Tyr36, Phe49, Tyr75, Tyr95, Trp108, and Phe113) and two polar residues (Lys32 and Ser63) (Figure 9A). The Pro1 residues are conserved among all known homologues of MIF and D-dopachrome tautomerase. Although there is a pocket at the N-terminal proline of D-dopachrome tautomerase similar to MIF, no aromatic residue, except His76, could be found near the cavity (Figure 9A). Most of those aromatic residues are substituted for by nonhydrophobic amino acids in D-dopachrome tautomerase (Figure 9B). Instead of these aromatic residues, the side chains of Arg36, Ser50, Leu96 Lys109, and Met114 are located on the surface of the N-terminal pockets of D-dopachrome tautomerase. On the other hand, Lys32 and Ser63, which are highly conserved on sequence alignment, have similar relative positions to Pro1, and they also have similar side chain conformations. Other conserved residues (Ala27, Lys32, Pro33, Ser63, Ile64, and Gly65) on the surface are also very close by the N-terminal proline. Considering these results, the conversion of D-dopachrome would be catalyzed in this pocket of

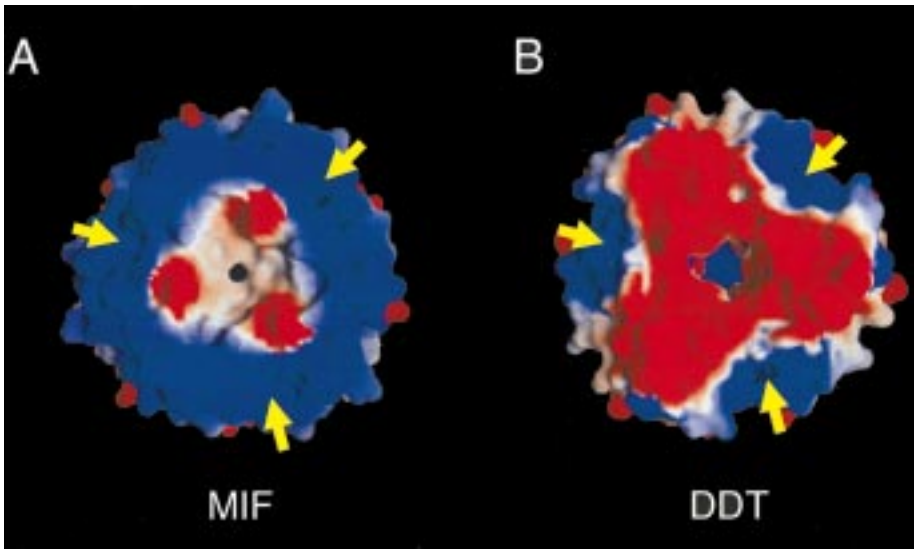

FIGURE 8: Electrostatic surface potential in D-dopachrome tautomerase and the human MIF trimer, as calculated by GRASP (*65*). Positively and negatively charged potentials are represented in blue and red, respectively. The two molecules are drawn in the same direction and viewed along the triad axis. Yellow arrows represent the potential active sites in N-terminal pockets. The orientations of these molecules are identical to those shown in Figure 7A,B. (A) Most of the surface on the portrayed side of MIF, including the potential active site, is positively charged. The regions around the 3-fold axis are noncharged. (B) On the other hand, a negatively charged surface of D-dopachrome tautomerase is widely distributed on the same side of MIF. Only the regions around the potential active site (yellow arrows) are positively charged, as in MIF.

D-dopachrome tautomerase as it is in MIF. The N-terminal proline and other conservative residues would thus be profoundly involved in the mechanism of D-dopachrome tautomerization. However, some significant substitutions, namely, K66V and Y36R, are also observed at the active site. Furthermore, residues Trp108 and Phe113 in the C-terminal region of MIF, which are included in the cluster of aromatic residues and form a structural element that faces toward the active site pocket, are also changed to Lys109 and Met114, respectively. Rosengren et al. reported that MIF is less active than D-dopachrome tautomerase in catalyzing the conversion of D-dopachrome. However, MIF shows more activity when converting D-dopachrome methyl ester (*23*). The substitutions mentioned above may be related to the determination of specificity and affinity to the substrates. For a precise speculation of the D-dopachrome tautomerization mechanism, we must await results from studies that address the tertiary structure of the protein−substrate complex.

The C-terminal region in the crystal structure of rat MIF is disordered (*18*), and the C-terminal-truncated mutants of human MIF lose the capacity for macrophage activation, suggesting that this region of human MIF and D-dopachrome tautomerase may have a flexible nature and may significantly affect cytokine activity and/or enzymatic reactions (*19*). However, the C-terminal region of human D-dopachrome tautomerase is tightly linked to the adjacent monomer by hydrogen bonds (Figure 5A). In the refined structure of human D-dopachrome tautomerase, the average temperature factors of the main chain and side chain atoms of residues 104−114, which comprise the two β-strands with a short hairpin, are 9.75 and 13.36 Å^2, respectively; these values are lower than the average value for all atoms of the protein (14.77 Å^2). Similarly, this region of human MIF has a normal temperature factor, and there is little difference between the three chains. Considering these results, this region does not appear to have significant flexibility in the C-terminal residues of human D-dopachrome tautomerase and MIF. However, in all of the cases discussed here, the structure of human MIF and D-dopachrome tautomerase reveals that many of the residues in this region are solvent accessible and some of the residues are located toward the active site pocket. Therefore, further study is necessary to clarify the role of C-terminal residues.

Comparison with CHMI and 4-OT. The monomer of D-dopachrome tautomerase, which is comprised of a two-layer α-β sandwich, somewhat resembles dimeric interleukin 8-like chemokines and the peptide binding domain of MHC (*43*, *44*). The barrel structure, which has 3-fold symmetry, is also observed in interleukin 1β, fibroblast growth factor, and tumor necrosis factor (*45*−*49*). However, the folding topology of MIF and D-dopachrome tautomerase, namely, two $\beta\alpha\beta$ units with 2-fold symmetry in a single polypeptide chain, is unlike that of any cytokine or hormones. The β-sheets pack around the 3-fold axis and do not form a barrel; the mixed β-sheet forms a trimer with three closely packed β-sheets.

MIF and D-dopachrome tautomerase show striking structural similarities to the bacterial enzymes CHMI and 4-OT (*22*). Both enzymes are involved in the degradation of aromatic compounds and catalyze keto−enol isomerization. Although in the primary sequence alignment CHMI shows only very limited homology with MIF and D-dopachrome tautomerase (Figure 1) and no significant homology with 4-OT, these four proteins have an almost identical subunit topology with the two $\beta\alpha\beta$ motifs related by pseudo-2-fold symmetry and trimeric β-sheet packing (Figures 6 and 7). While CHMI exists as a homotrimer, 4-OT is a hexamer. The 4-OT monomer is composed of 62 amino acids and is dimerized by 2-fold symmetry to form a structure similar to that of the D-dopachrome tautomerase monomer. Therefore, 4-OT is a trimer of the homodimer that shows 32 symmetry; its overall tertiary structure is very similar to the trimer structure of MIF, D-dopachrome tautomerase, and CHMI.

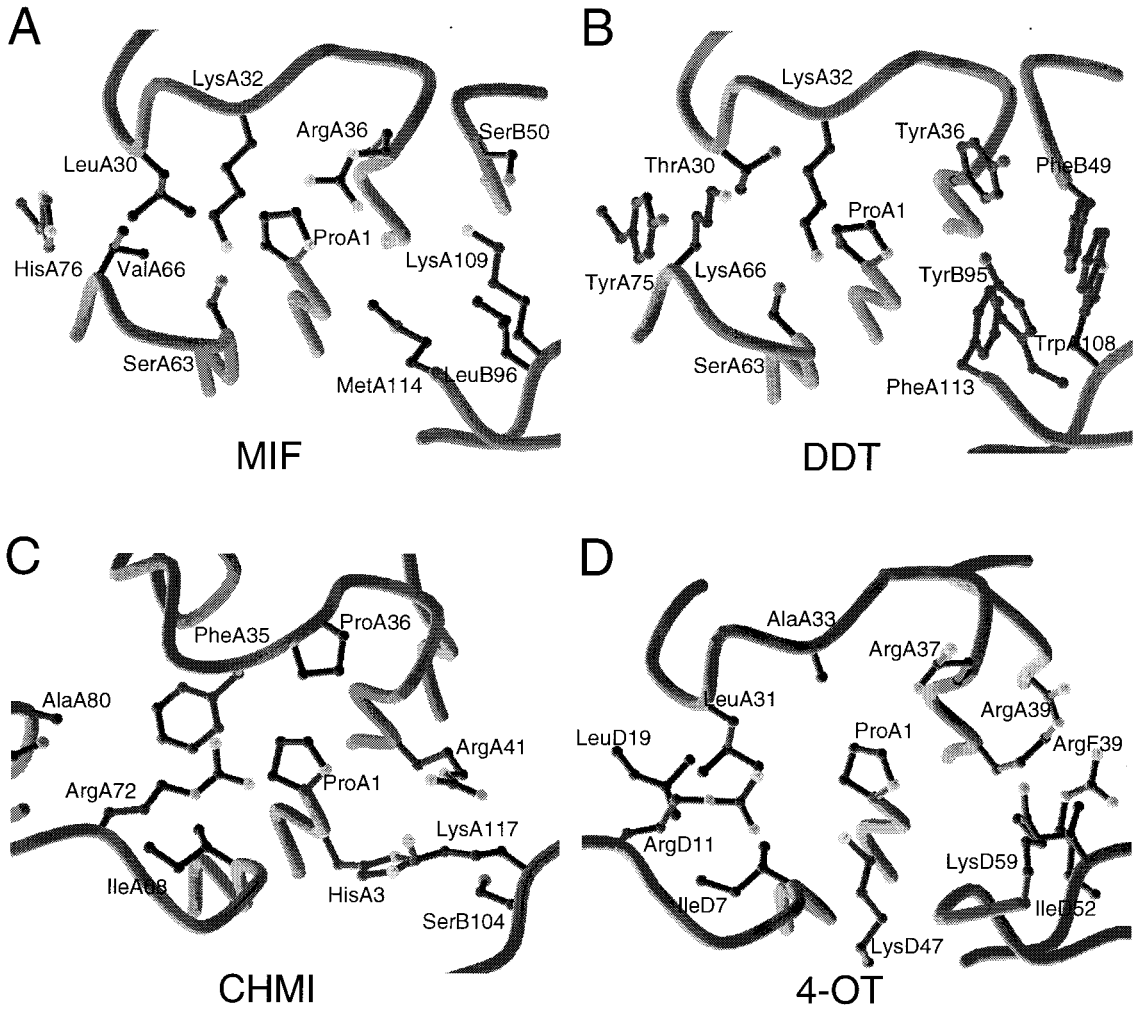

FIGURE 9: Putative active sites at the N-terminal proline. The main chains are represented by tubes. The side chains around the active site are shown in a ball-and-stick representation. (A) The N-terminal proline of human MIF is surrounded by a large number of aromatic residues (Tyr36, Phe49, Tyr75, Tyr95, Trp108, and Phe113). (B) The conversion of D-dopachrome would be catalyzed in this pocket in D-dopachrome tautomerase. Although there are pockets at the N-terminal proline, no aromatic residue, except His76, could be found around the pockets. Most of the residues located on the surface of the N-terminal cavity were nonaromatic amino acids, Arg36, Ser50, Leu96, Lys109, and Met114, in D-dopachrome tautomerase. However, the relative positions of the highly conserved side chains, Pro1, Lys32, and Ser63, and their torsion angles are very similar to those shown in (A). (C) Three Arg residues exist in the catalytic pocket of CHMI (PDB code 1otg). (D) The catalytic pocket of 4-OT (PDB code 1otf). The side chains of Arg39, Arg61, and Arg61 and backbone atom of Ser37 are involved in the interaction with the adduct 2-OP. These figures were prepared with MOLSCRIPT (*62*) and RASTER3D (*63*).

CHMI and 4-OT possess active site pockets on the surface near the N-terminal proline, which are utilized as a catalytic base in their isomerization reactions. There are only 19 identical residues (17%) between D-dopachrome tautomerase and CHMI. 4-OT shows no primary sequence homology with MIF and D-dopachrome tautomerase.

In regard to the main chain structure, CHMI monomers and 4-OT dimers are less similar to human D-dopachrome tautomerase monomers than is MIF. When the 27 α-carbon atoms in strands β1, β2, β4, and β5 (residues 2−7, 38−42, 57−64, and 95−102) of the D-dopachrome tautomerase monomer and 3 × 27 α-carbons of the trimer are superimposed with the structurally corresponding atoms (residues 3−8, 41−45, 62−69, and 103−110) in the CHMI monomer and trimer, the rms difference is less than 0.88 and 1.32 Å, respectively (Figure 6B). The greatest difference between the structures is found in the loop regions (particularly β1-α1, β3-β4, and α2-β5 and the C-terminal loop). Because of several insertion residues in CHMI, the orientation of the two α-helices with respect to that of the β-sheet is different between the two molecules. The surface shape of the active site pocket is also quite different from that of D-dopachrome tautomerase.

A superposition of 27 α-carbon atoms in the D-dopachrome tautomerase monomer on the 4-OT dimer (residues 3−8, 40−44, 2−9, and 39−46) and 3 × 27 atoms in the D-dopachrome tautomerase trimer on the 4-OT hexamer results in rms differences of 0.72 and 1.11 Å (Figure 6C), respectively. These values are not much larger than those existing between D-dopachrome tautomerase and MIF.

Subramanya et al. analyzed crystal structures and proposed a mechanism for reactions that are catalyzed by CHMI and 4-OT. These enzymes appear to operate via an analogous one-base mechanism having chemically similar unsaturated ketones as a substrate. In brief, the substrate [5-(carboxymethyl)-2-hydroxymuconate] for CHMI binds to the active site pocket such that the carboxylate group of substrate interacts with the side chains of Arg41 and Arg72 (Figure 9C). Then the N-terminal proline could remove the proton from the carbon with an electronic rearrangement of the substrate. In

4-OT, the two arginine residues correspond to Arg39 and Arg11 and locate at similar positions in the N-terminal pocket (Figure 9D). The crystal structure of 4-OT from *Pseudomonas putida* mt-2, which is inactivated by 2-oxo-3-pentynoate (2-OP), shows a covalent bond between C-4 of the adduct and Pro1 (*50*). In the complex structure, the Nϵ and Nη atoms of Arg39 from the neighboring dimer interact with the carbonyl and carboxylate oxygens in the adduct, respectively. The Nη atom of Arg61 from the same dimer also interacts with this carboxylate oxygen in the adduct. The Nϵ atom of the Arg61 side chain interacts with the other carboxylate oxygen. In addition to these side chains, a water molecule bridges from the backbone atom of Ser37 and side chain of Arg39 to the C-2 keto group of the adduct by a hydrogen bond. These residues connect to the substrate for stabilization. However, Arg11 does not interact with the adduct. A comparison of the 2-OP−4-OT structure with other proteins provides an insight into the reaction mechanisms that are catalyzed by MIF and D-dopachrome tautomerase, because the enzymatic activity of not only 4-OT but also MIF is interrupted by an analogous 3-bromopyruvate (3-BP) that would be attached to Pro1 (*51*, *52*). When a detailed structural comparison of catalytic pockets is made, all of these proteins (D-dopachrome tautomerase, MIF, CHMI, and 4-OT) show positively charged properties in the active site pockets; they each have at least two positively charged residues on the pocket (Figure 9). However, it should be noted that these residues are not necessarily conserved. The Arg39 and Arg61 that form hydrogen bonds with an adduct in the crystal structure of 4-OT correspond to the Arg 41 and Lys117 in CHMI. While Arg36 and Lys109 of D-dopachrome tautomerase might serve as the Arg39 and Arg61 of 4-OT, only aromatic clusters are found in this region of MIF. In turn, Lys32 or/and Lys66 might play a role of substrate binding of MIF. Since the side chain environment of the catalytic pocket in D-dopachrome tautomerase is more similar to that of 4-OT than of MIF, we could presume that it can potentially interact with 3-BP or 2-OP. Some space remains left for those adducts between side chains of Arg36 and Lys109 in the catalytic pocket of D-dopachrome tautomerase (Figure 9B).

Biological Aspects. On the basis of their sequence homology and similar enzyme activity, it has been speculated that interesting structural features might be discovered between D-dopachrome tautomerase and the trimeric structure of MIF; however, the precise structure of D-dopachrome tautomerase has been unclear to this point. In the present study, we determined the high-resolution structure of human D-dopachrome tautomerase, which clearly shows that although there are similarities in the overall main chain structure, there remain several significant differences between the two proteins. A precise comparison is expected to provide a major clue in the investigation of the potential of D-dopachrome tautomerase as a cytokine or a pluripotent bioactive molecule.

It has been reported that MIF secreted from immune cells plays an important role in the initialization of inflammatory reactions and cytokine production and is secreted from the pituitary gland, much like a hormone, in response to LPS stimulation (*7*, *9*, *10*). In cases of infection, D-dopachrome tautomerase may function in concert with MIF. A report by Esumi et al. presents evidence that the genes for D-dopachrome tautomerase and MIF are closely linked and that they have a conserved structure (*53*). Northern blot analysis has demonstrated that mRNA of D-dopachrome tautomerase is expressed in large amounts in the liver and to a lesser extent in other organs, including the heart and spleen (*26*). In contrast, MIF mRNA is largely expressed in the brain and kidneys and to an even lesser extent in the liver. This indicates that the biological action of D-dopachrome tautomerase might be limited mainly, or completely, to the liver, in contrast to the broad spectrum of functions performed by MIF. In any case, further evaluation of the action of D-dopachrome tautomerase is necessary. Wistow et al. reported that epithelial cells of chicken embryonic lens expressed this protein (*12*). We found that MIF is abundantly expressed in the proliferative basal cell layers of the epidermis and also in the endothelial and epithelial cells of the cornea, suggesting that MIF might be involved in cell growth or differentiation. From these findings, we are currently investigating the actual biological functions of D-dopachrome tautomerase in the events of immune responses as well as cell proliferation and differentiation.

Furthermore, MIF is also reported to exhibit enzymatic oxidoreductase activity in the presence of GSH as a reducing agent (*54*). It is also reported that the mutant C59S is completely inactive and that C56S is partly active in both the oxidoreductase and the macrophage-activating functions (*55*). It is not clear whether D-dopachrome tautomerase also possesses oxidoreductase activity. In the crystal structure of MIF, the residue Cys59, the putative catalytic center of oxidoreductase, is buried in the hydrophobic core between helices and the β-sheet, and Cys56 is not completely buried. In contrast, Cys59 is substituted to Leu in D-dopachrome tautomerase, and Cys56 is buried in the side chains of the surrounding residues. These results indicate that D-dopachrome tautomerase is unlikely to possess the same enzymatic oxidoreductase activity as does MIF.

In addition to its roles as D-dopachrome tautomerase, phenylpyruvate tautomerase, and oxidoreductase, MIF has an affinity for *S*-hexylglutathione and is reported to show GST activity as well (*56*, *57*). D-Dopachrome tautomerase is not retained by *S*-hexylglutathione−agarose as MIF. MIF and GST share no structural similarities. In addition, evolutionary relationships are improbable. However, it is of note that D-dopachrome tautomerase and Theta-class GST genes have been shown by Coggan et al. to be duplicated in an inverted repeat (*58*).

The biological importance of isomerase activity remains unknown. Recently, it has been reported that MIF catalyzes isomerization of a phenyl pyruvate other than D-dopachrome; however, due to its low affinity to the enzyme, this molecule may not be the true substrate. In regard to the role of cytokine activity in relation to isomerase activity, it is known that cyclophilin, a cyclosporin-binding protein, possesses peptidyl−prolyl cis−trans isomerase activity (*59*). Cyclophilin is a soluble cytosolic protein and is present in high concentrations in many mammalian tissues. It is of interest that cyclophilin is secreted by macrophages in response to endotoxin in a manner similar to MIF and that it exhibits proinflammatory activity (*60*). In this context, it is thought that such isomerase activity is critical for immune responses. Therefore, it is still possible that D-dopachrome tautomerase and MIF might both be involved in the immune response through isomerization of certain other substrates. A recent

report about a MIF mutant also reveals the significance of Pro1 in both enzymatic reactions and neutrophile activation (*25*). Accordingly, the roles of the N-terminal pocket and Pro1 in catalysis and cytokine activity clearly need to be determined for further understanding of the biological function of MIF and D-dopachrome tautomerase. The present structural analysis of D-dopachrome tautomerase offers a novel approach for the design of inhibitors that modulate immunoregulatory and hormone-like effects. This study would also benefit attempts to develop further therapeutic approaches.

ACKNOWLEDGMENT

We thank Professor N. Sakabe, Dr. N. Watanabe, and Dr. M. Suzuki for their help in data collection at the Photon Factory. The experiments using synchrotron radiation were performed under the approval of the Photon Factory admission committee, KEK, Japan (PAC No. 97G087).

REFERENCES

1. Odh, G., Hindemith, A., Rosengren, A. M., Rosengren, E., and Rorsman, H. (1993) *Biochem. Biophys. Res. Commun. 197*, 619−624.
2. Yokoyama, K., Yasumoto, K., Suzuki, H., and Shibahara, S. (1994) *J. Biol. Chem. 269*, 27080−27087.
3. Zhang, M., Aman, P., Grubb, A., Panagopoulos, I., Hindemith, A., Rosengren, E., and Rorsman, H. (1995) *FEBS Lett. 373*, 203−206.
4. Weiser, W. Y., Temple, P. A., Witek-Giannotti, J. S., Remold, H. G., Clark, S. C., and David, J. R. (1989) *Proc. Natl. Acad. Sci. U.S.A. 86*, 7522−7526.
5. Bloom, B. R., and Bennett, B. (1966) *Science 153*, 80−82.
6. David, J. R. (1966) *Proc. Natl. Acad. Sci. U.S.A. 56*, 72−77.
7. Bernhagen, J., Calandra, T., Mitchell, R. A., Martin, S. B., Tracey, K. J., Voelter, W., Manogue, K. R., Cerami, A., and Bucala, R. (1993) *Nature 365*, 756−759.
8. Bernhagen, J., Bacher, M., Calandra, T., Metz, C. N., Doty, S. B., Donnelly, T., and Bucala, R. (1996) *J. Exp. Med. 183*, 277−282.
9. Bucala, R. (1994) *Immunol. Lett. 43*, 23−26.
10. Bucala, R. (1996) *FASEB J. 10*, 1607−1613.
11. Calandra, T., Bernhagen, J., Metz, C. N., Spiegel, L. A., Bacher, M., Donnelly, T., Cerami, A., and Bucala, R. (1995) *Nature 377*, 68−71.
12. Wistow, G. J., Shaughnessy, M. P., Lee, D. C., Hodin, J., and Zelenka, P. S. (1993) *Proc. Natl. Acad. Sci. U.S.A. 90*, 1272−1275.
13. Matsuda, A., Kotake, S., Tagawa, Y., Matsuda, H., and Nishihira, J. (1996) *Immunol. Lett. 53*, 1−5.
14. Matsuda, A., Tagawa, Y., Matsuda, H., and Nishihira, J. (1996) *FEBS Lett. 385*, 225−228.
15. Onodera, S., Suzuki, K., Matsuno, T., Kaneda, K., Kuriyama, T., and Nishihira, J. (1996) *Immunology 89*, 430−435.
16. Shimizu, T., Ohkawara, A., Nishihira, J., and Sakamoto, W. (1996) *FEBS Lett. 381*, 199−202.
17. Hirokawa, J., Sakaue, S., Tagami, S., Kawakami, Y., Sakai, M., Nishi, S., and Nishihira, J. (1997) *Biochem. Biophys. Res. Commun. 235*, 94−98.
18. Suzuki, M., Sugimoto, H., Nakagawa, A., Tanaka, I., Nishihira, J., and Sakai, M. (1996) *Nat. Struct. Biol. 3*, 259−266.
19. Sugimoto, H., Suzuki, M., Nakagawa, A., Tanaka, I., Nishihira, J., and Sakai, M. (1996) *FEBS Lett. 389*, 145−148.
20. Sun, H. W., Bernhagen, J., Bucala, R., and Lolis, E. (1996) *Proc. Natl. Acad. Sci. U.S.A. 93*, 5191−5196.
21. Kato, Y., Muto, T., Tomura, T., Tsumura, H., Watarai, H., Mikayama, T., Ishizaka, K., and Kuroki, R. (1996) *Proc. Natl. Acad. Sci. U.S.A. 93*, 3007−3010.
22. Subramanya, H. S., Roper, D. I., Dauter, Z., Dodson, E. J., Davies, G. J., Wison, K. S., and Wigley, D. B. (1996) *Biochemistry 35*, 792−802.
23. Rosengren, E., Bucala, R., Aman, P., Jacobsson, L., Odh, G., Metz, C. N., and Rorsman, H. (1996) *Mol. Med. 2*, 143−149.
24. Rosengren, E., Aman, P., Thelin, S., Hansson, C., Ahlfors, S., Bjork, P., Jacobsson, L., and Rorsman, H. (1997) *FEBS Lett. 417*, 85−88.
25. Swope, M., Sun, H.-W., Blake, P. R., and Lolis, E. (1998) *EMBO J. 17*, 3534−3541.
26. Nishihira, J., Fujinaga, M., Kuriyama, T., Suzuki, M., Sugimoto, H., Nakagawa, A., Tanaka, I., and Sakai, M. (1998) *Biochem. Biophys. Res. Commun. 243*, 538−544.
27. Sugimoto, H., Taniguchi, M., Nakagawa, A., Tanaka, I., Suzuki, M., and Nishihira, J. (1997) *J. Struct. Biol. 120*, 105−108.
28. Sakabe, N., Ikemizu, S., Sakabe, K., Higashi, T., Nakagawa, A., Watanabe, N., Adachi, S., and Sasaki, K. (1995) *Rev. Sci. Instrum. 66*, 1276−1281.
29. Otwinowski, Z. (1993) in *Daresbury Study Weekend Proceedings* (Wolf, W., Evans, P. R., and Leslie, A. G. W., Eds.) pp 80−86, SERC Daresbury Laboratory, Warrington, U.K.
30. Collaborative Computational Project, Number 4 (1994) *Acta Crystallogr. D50*, 760−763.
31. Navaza, J. (1994) *Acta Crystallogr. A50*, 157−163.
32. Kleywegt, G. J. (1996) *ESF/CCP4 Newsl. 32*, 32−36.
33. Brünger, A. T. (1993) *X-PLOR: Version 3.1. A System for X-ray Crystallography and NMR*, Yale University Press, New Haven, CT.
34. Brünger, A. T., Kuriyan, J., and Karplus, M. (1987) *Science 235*, 458−460.
35. Brünger, A. T., Krukowski, A., and Erickson, J. (1990) *Acta Crystallogr. A46*, 585−593.
36. Brünger, A. T. (1992) *Nature 355*, 472−475.
37. Jones, T. A., Zou, J. Y., Cowan, S. W., and Kjeldgaard, M. (1991) *Acta Crystallogr. A47*, 110−119.
38. Jiang, J.-S., and Brünger, A. T. (1994) *J. Mol. Biol. 243*, 100−115.
39. Laskowski, R. A., MacArthur, M. W., Moss, D. S., and Thornton, J. M. (1993) *J. Appl. Crystallogr. 26*, 283−291.
40. Hooft, R. W. W., Vriend, G., Sander, C., and Abola, E. E. (1996) *Nature 381*, 272.
41. Luzzati, P. V. (1952) *Acta Crystallogr. 5*, 802−810.
42. Yoshida, H., Nishihira, J., Suzuki, M., and Hikichi, K. (1997) *Biochem. Mol. Biol. Int. 42*, 891−899.
43. Baldwin, E. T., Weber, I. T., St. Charles, R., Xuan, J. C., Appella, E., Yamada, M., Matsushima, K., Edwards, B. F., Clore, G. M., Gronenborn, A. M., and et al. (1991) *Proc. Natl. Acad. Sci. U.S.A. 88*, 502−506.
44. Garboczi, D. N., Ghosh, P., Utz, U., Fan, Q. R., Biddison, W. E., and Wiley, D. C. (1996) *Nature 384*, 134−141.
45. Priestle, J. P., Schar, H. P., and Grutter, M. G. (1989) *Proc. Natl. Acad. Sci. U.S.A. 86*, 9667−9671.
46. Finzel, B. C., Clancy, L. L., Holland, D. R., Muchmore, S. W., Watenpaugh, K. D., and Einspahr, H. M. (1989) *J. Mol. Biol. 209*, 779−791.
47. Zhang, J. D., Cousens, L. S., Barr, P. J., and Sprang, S. R. (1991) *Proc. Natl. Acad. Sci. U.S.A. 88*, 3446−3450.
48. Zhu, X., Komiya, H., Chirino, A., Faham, S., Fox, G. M., Arakawa, T., Hsu, B. T., and Rees, D. C. (1991) *Science 251*, 90−93.
49. Banner, D. W., D'Arcy, A., Janes, W., Gentz, R., Schoenfeld, H. J., Broger, C., Loetscher, H., and Lesslauer, W. (1993) *Cell 73*, 431−445.
50. Taylor, A. B., Czerwinski, R. M., Johnson, W. H. J., Whitman, C. P., and Hackert, M. L. (1998) *Biochemistry 37*, 14692−14700.
51. Stamps, S. L., Fitzgerald, M. C., and Whitman, C. P. (1998) *Biochemistry 37*, 10195−10202.
52. Stivers, J. T., Abeygunawardana, C., Mildvan, A. S., Hajipour, G., Whitman, C. P., and Chen, L. H. (1996) *Biochemistry 35*, 803−813.
53. Esumi, N., Budarf, M., Ciccarelli, L., Sellinger, B., Kozak, C. A., and Wistow, G. (1998) *Mamm. Genome 9*, 753−757.
54. Kleemann, R., Mischke, R., Kapurniotu, A., Brunner, H., and Bernhagen, J. (1998) *FEBS Lett. 430*, 191−196.

55. Kleemann, R., Kapurniotu, A., Frank, R. W., Gessner, A., Mischke, R., Flieger, O., Juttner, S., Brunner, H., and Bernhagen, J. (1998) *J. Mol. Biol. 280*, 85−102.
56. Blocki, F. A., Schlievert, P. M., and L. P., W. (1992) *Nature 360*, 269−270.
57. Blocki, F. A., Ellis, L. B. M., and Wackett, L. P. (1993) *Protein Sci. 2*, 2095−2102.
58. Coggan, M., Whitbread, L., Whittington, A., and Board, P. (1998) *Biochem. J. 334*, 617−623.
59. Takahashi, N., Hayano, T., and Suzuki, M. (1989) *Nature 337*, 473−475.
60. Sherry, B., Yarlett, N., Strupp, A., and Cerami, A. (1992) *Proc. Natl. Acad. Sci. U.S.A. 89*, 3511−3515.
61. Read, R. J. (1986) *Acta Crystallogr. A42*, 140−149.
62. Kraulis, P. J. (1991) *J. Appl. Crystallogr. 24*, 946−950.
63. Merritt, E. A., and Bacon, D. J. (1997) *Methods Enzymol. 277*, 505−524.
64. Evans, S. V. (1993) *J. Mol. Graphics 11*, 134−138.
65. Nicholls, A., Sharp, K., and Honig, B. (1991) *Proteins 11*, 281−296.

BI982184O